J. Chem. Sci. Vol. 128, No. 3, March 2016, pp. 339–347.
DOI 10.1007/s12039-016-1034-z

On the electrocatalytic activity of nitrogen-doped reduced graphene Oxide: Does the nature of nitrogen really control the activity towards oxygen reduction?

SOURAV BAG and C RETNA RAJ*
Functional Materials and Electrochemistry Laboratory, Department of Chemistry,
Indian Institute of Technology Kharagpur, Kharagpur 721 302, India
e-mail: crraj@chem.iitkgp.ernet.in

MS received 7 July 2015; revised 7 September 2015; accepted 5 October 2015

Abstract. Synthesis of metal-free electrocatalyst for the cathodic reduction of oxygen is of great interest for fuel cell and metal-air battery applications. The heteroatom-doped graphene/reduced graphene oxide (rGO) is very promising and the nitrogen-doped rGO (N-rGO) is emerging as a new inexpensive electrocatalyst for oxygen reduction reaction (ORR). Herein, we describe the effect of the chemical nature and amount of nitrogen in N-rGO towards ORR in acidic solution. Four different samples of N-rGO with different nitrogen content were synthesized by simple chemical route. The chemical nature and nitrogen content were analyzed with X-ray photoelectron spectroscopic measurements. The electrocatalytic performance of the catalyst was examined by cyclic and hydrodynamic voltammetric studies. All the N-rGO samples favor 4-electron pathway for the reduction of oxygen in acidic solution. The onset potential and kinetic current density depends on the nature of the doped nitrogen. It is demonstrated that the chemical nature and the amount of nitrogen actually control the ORR activity. The N-rGO which contains a large amount of pyridinic nitrogen with N/C ratio of 0.074 has high catalytic activity. The carbon bonded to pyridinic nitrogen could be a possible catalytic site in ORR. Our studies suggest that the graphitic nitrogen does not significantly influence the electrocatalytic activity of N-rGO.

Keywords. Reduced graphene oxide; nitrogen doping; electrocatalysis; oxygen reduction reaction.

1. Introduction

Oxygen reduction reaction (ORR) is one of the most extensively studied electrochemical reactions for fuel cell and metal-air battery applications. Oxygen can be reduced to water in aqueous medium via two different pathways: (i) 2-step 2-electron (peroxide pathway) and (ii) direct 4-electron pathways. The mechanism of ORR largely depends on the nature of the electrode, solution pH, solvent, etc. The catalyst that favors the 4-electron pathway for ORR is critically required for fuel cell and metal-air batteries. Traditionally, Pt has been used as a cathode catalyst in polymer electrolyte membrane fuel cells. Pt is known to favor 4–electron pathway in acidic and alkaline pH. However, the high cost, lack of durability and poor electron transfer kinetics limits the use of Pt for practical application. Moreover, in the membrane electrode assembly of fuel cell, the carbon supported Pt catalysts are not effectively used in the catalysis as most of the catalysts are buried inside the pores of carbon. A high surface area catalyst support, inexpensive and durable electrocatalysts are critically required for fuel cell applications. Skillful design of less expensive metal-free or non-Pt catalyst without compromising the electrocatalytic activity is a promising approach to increase the performance and to decrease the overall cost of the fuel cell. Although, several attempts have been made in the past to develop such catalyst, still it is a challenging task to achieve high current density and durability with these catalysts.[1–4] The non-precious metals and transition metal oxides have been suggested as alternate electrocatalysts for ORR.[3–5] Although, these catalysts are considered to be cost-effective, they do not promote the 4-electron pathway for ORR in acidic solution and their poor catalytic activity limits their practical applications.

Recently, the metal-free carbon-based materials have emerged as efficient catalysts for ORR.[6,7] Carbon nanotubes (CNTs) and one atom thick graphene have attracted considerable attention owing to their unique mechanical and electronic properties. The large specific surface area, high electronic and thermal conductivity of graphene make it as an ideal candidate for various electrocatalytic applications. CNTs and graphene have

*For correspondence

Dedicated to Professor R. Ramaraj on the occasion of his 60th birth anniversary.

also been used as catalyst supports for various electrocatalytic reactions.[2,3,8,9] The electronic properties of graphene can be effectively further tailored by doping with heteroatoms like nitrogen, boron, sulfur, etc. The doping of graphene or reduced graphene oxide (rGO) has been achieved by chemical vapour deposition, arc-discharge, hydrothermal, etc., methods.[10–13] The heteroatoms have been doped either on the basal plane or at the edges of rGO sheets. Such doping is known to impart interesting properties on the honeycomb carbon network. These heteroatom doped carbon networks have been exploited for catalytic, sensing, etc., applications.[11–19] For instance, recent studies show that the nitrogen-doped graphene and carbon nanotube have good electrocatalytic activity and they have been considered as an efficient metal-free catalyst for oxygen reduction reaction (ORR).[11–17] The electrocatalytic activity of these metal-free catalysts are claimed to be better than or equivalent to that of the conventional Pt/C catalyst, although the actual catalytic mechanism is not well understood. Though several papers have been published on the electrocatalytic activity of nitrogen-doped graphene, the actual mechanism involved in ORR and the active site of the catalyst are not well established. The doped nitrogen is believed to play a key role in regulating the electrocatalytic performance of rGO towards ORR. Does the electronic nature of nitrogen on rGO and nitrogen content really matter in the electrocatalytic performance? What type of nitrogen is more active towards ORR? Nitrogen-doped rGO (N-rGO) containing different types and varying amount of nitrogen were synthesized[20,21] using single source reducing/doping agent and explored the catalytic performance to answer these questions. Herein, we describe the synthesis of N-rGO containing varying amount of nitrogen and its electrocatalytic activity towards ORR in acidic solution. We demonstrate that the nature of nitrogen and nitrogen content actually control the electrocatalytic activity of N-rGO.

2. Experimental

2.1 *Materials and reagents*

Graphite and hydrazine hydrate were purchased from Sigma Aldrich. NH_3, $NaNO_3$, $KMnO_4$, H_2SO_4 and all the other chemicals were obtained from Merck India. All the solutions were made with Millipore water (Milli Q system).

2.2 *Exfoliation of graphite and synthesis of GO*

GO was synthesized according to our earlier procedure[3,4,22,23] based on Hummer's method[24] by the exfoliation of graphite. Briefly, graphite powder (1 g) was mixed with concentrated H_2SO_4 (50 mL) and $NaNO_3$ (1 g) in a 500 mL round-bottom flask at 0°C. Then solid $KMnO_4$ (6 g) was added to the reaction mixture and it was stirred continuously for 1 h at room temperature. The reaction mixture was then diluted with 200 mL of water. After 15 min, 30% H_2O_2 solution (∼5 mL) was added to the reaction vessel until the gas evolution ceased. The exfoliated graphite was then separated from the reaction mixture by centrifugation process. The residue was then washed thoroughly with 5% HCl solution. The washing was continued until the supernatant gave a negative test for the sulfate ions with aqueous $BaCl_2$ solution. The yellow-brown residue obtained after repeated washing with HCl was further washed with copious amounts of Millipore water and dried in vacuum.

2.3 *Synthesis of N-rGOs*

In a typical procedure, 20 mg of GO was dispersed in 40 mL of water in a round bottom flask by ultrasonication for 1 h. Then 200 μL of 25% NH_3 solution was added into the GO dispersion and the pH of the reaction mixture was maintained between 9 and 10. Required amount of hydrazine hydrate (99%, 1.03 mg/mL) was then added to the reaction mixture and refluxed at a temperature of 95°C for 3 h. Then the mixture was centrifuged and washed thoroughly with copious amount of water and alcohol and dried at 150°C in vacuum oven. Hereafter the product obtained with different concentration of hydrazine hydrate, 0.01, 0.02 0.05 and 0.1 mM, are referred to as N-rGO1, N-rGO2, N-rGO3 and N-rGO4, respectively. The undoped rGO was synthesized by refluxing 20 mg GO in 20 mL ethylene glycol at 180°C for 3 h.[4]

2.4 *Electrode preparation*

The glassy carbon (GC) rotating disk (RDE) and GC-Pt rotating ring-disk electrodes (RRDE) were polished well with fine emery paper and alumina (0.05 μm) slurry and sonicated in Millipore water for 10-15 min to remove the physically adsorbed impurities. These electrodes were washed repeatedly with copious amount of Millipore water and dried.The catalyst ink was prepared by mixing the as-synthesized materials (0.4 mg) with 200 μL Nafion (1%) in ethanol and sonicating it for an hour. An aliquot of the catalyst ink was drop-cast on the surface of the electrode and dried at room temperature. The mass of the catalyst on the electrode surface was kept at 0.1 mg/cm^2.

2.5 *Instrumentation*

The surface morphology of the catalyst was examined with JEOL JEM 2010 transmission electron microscope (TEM) at an operating voltage of 200 kV and FEI NOVA NANOSEM 450 field emission scanning electron microscope (FESEM). Energy dispersive X-ray microanalyzer (BRUKER EDAX) attached to the electron microscope was used for elemental compositional analysis of the catalyst. FTIR analysis was carried out with Perkin Elmer Spectrum 1 RX 1 FTIR spectrometer. The X-ray photoelectron spectroscopic (XPS) measurements were carried out with PHI 5000 versaprobe II scanning XPS microscope using the energy source Al (Kα, hν = 1486.6 eV). XPS data were deconvoluted and analyzed using XPS peak-fit software. Raman spectroscopic measurement was performed using a Jobin Yvon Horiba T64000 spectrometer (France) with an excitation source of Argon-Krypton mixed ion gas laser (514 nm, Spectra Physics, USA). Electrochemical experiments were done in a two-compartment, three-electrode cell with Ag/AgCl (3M KCl) reference, a Pt wire auxiliary and GC rotating disk (RDE) and GC disk-Pt ring rotating-ring-disk (RRDE) working electrodes. Autolab potentiostat-galvanostat (302 N) workstation with computer controlled GPES software and PINE electrode rotating instruments (USA) were used in the electrochemical studies. All the potential value is referred against the reversible hydrogen electrode (RHE). The Ag/AgCl (3M KCl) reference electrode was calibrated using the standard procedures (figure S1 in Supplementary Information, SI).[25]

3. Results and Discussion

3.1 *Synthesis and characterization*

Scheme 1 illustrates the chemical route for the reduction of graphene oxide (GO) and nitrogen doping onto the rGO framework. Reduction of GO and nitrogen doping were achieved in single-step with single reagent, hydrazine hydrate. The FTIR spectral measurements show a remarkable decrease in the intensity of the peaks corresponding to the stretching of oxygen containing functionalities such as C=O (1720 cm^{-1}), epoxy C-O (1227 cm^{-1}), carboxylic C-O (1320–1210 cm^{-1}), alkoxy C–O (1050 cm^{-1}), O–H stretching (3400 cm^{-1}) and O–H deformation vibrations (1410 cm^{-1}) (figure 1a).[22,23] The intense peak at 800 cm^{-1} is attributed to C-H bending vibration; gradual increase in the intensity of this band was noticed while increasing the amount of reducing agent in the reaction vessel (from N-rGO1 to N-rGO4) due to the gradual recovery of C-H bond at the periphery of rGO framework.[26] A careful examination of the FTIR spectral profile (figure 1a) reveals that the characteristic signature for the oxygen containing functional groups steadily decreases from N-rGO1 to N-rGO4; the peaks vanished in the case of N-rGO4, implying the effective removal of oxygen functionalities by hydrazine. A new peak attributed to the skeletal vibration of graphene was noticed at 1580 cm^{-1}.[22,26] Moreover, the characteristic C-N stretching vibration was observed at 1000, 1100 and1270 cm^{-1}.[27–29] The Raman spectra of GO (figure 1b) show characteristic D and G bands at 1350 and 1600 cm^{-1}, respectively.[12] The D band is due to the structural defects whereas the G band is associated with the E_{2g} mode of sp^2 carbon domain in the rGO network. The integrated intensity ratio of the D and G bands in GO is 0.89 and it gradually increases to 1.18 while moving from N-rGO1 to N-rGO4. The intensity ratio can be taken as an indication of relative disorder present in the carbon network.[20,30,31] The increase in the ratio suggests the presence of defects associated with nitrogen doping and decrease in the average size of sp^2 domain.[20,30,31] Furthermore, as can be seen in figure 1b, gradual red shift of D band position was observed while moving from N-rGO1 to N-rGO4. Such a shift may be ascribed to the presence of defects or strain effect due to doping, though the actual reason for such shift is not clearly understood at the present stage.

Figure 2 displays the TEM images of N-rGO3 and selected area electron diffraction (SAED) pattern. The spotty SAED pattern in the inset (figure 2a) reveals the single crystalline nature of the N-rGO3 sheet. The FESEM image and the corresponding elemental mapping and EDX analysis confirm the presence of nitrogen, carbon and oxygen (figure S2). The XPS analysis supports the reduction of GO and the doping of nitrogen atom onto the rGO framework. The XPS surface survey scan of all N-rGOs shows characteristic signature for C, O and N (figure S3).The deconvoluted C1s spectra of GO shows three peaks at 284.34, 286.4 and 288.5eV corresponding to C-C, C-O (epoxy, hydroxyl, etc.) and carboxyl (-O=C-O-) functions of GO, respectively (figure S4A).[11,26] The removal of oxygen functionalities and the graphitization of the carbon network is clearly seen in the deconvoluted C1s spectral profiles of N-rGOs. As we move from N-rGO1 to N-rGO4 the intensity of the peak corresponding to the oxygen functionalities decreases with a concomitant increase in the intensity of the peak at 284.34 eV corresponding to the sp^2 C-C bond. It suggests the efficient removal of oxygen functionalities and the recovery sp^2 carbon at high concentration of hydrazine hydrate. In order to

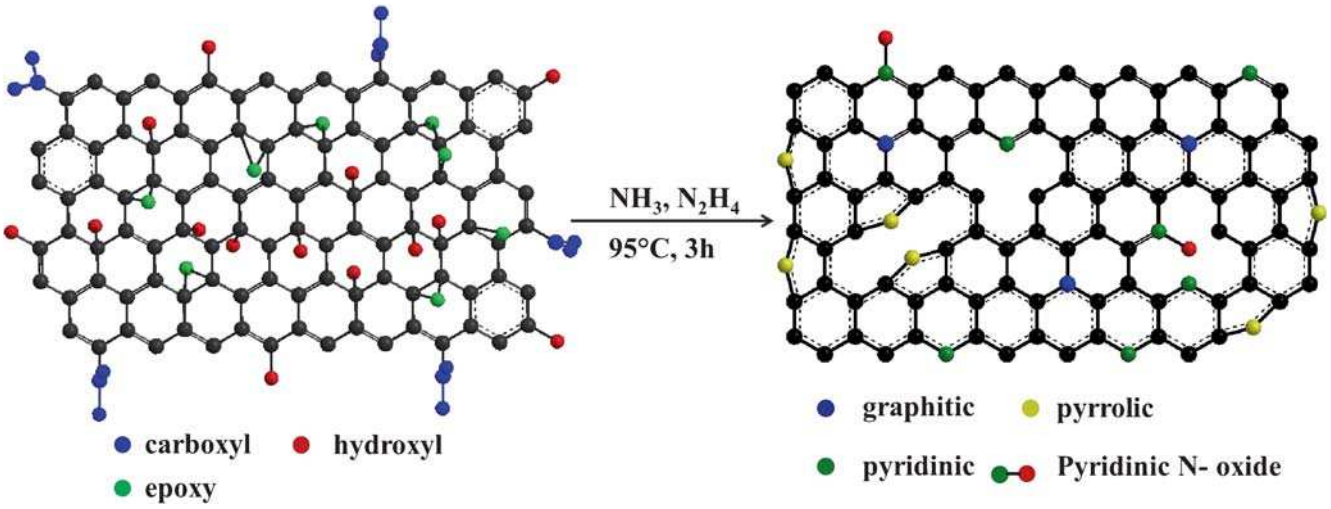

Scheme 1. Schematic illustration of the synthesis of N-rGO.

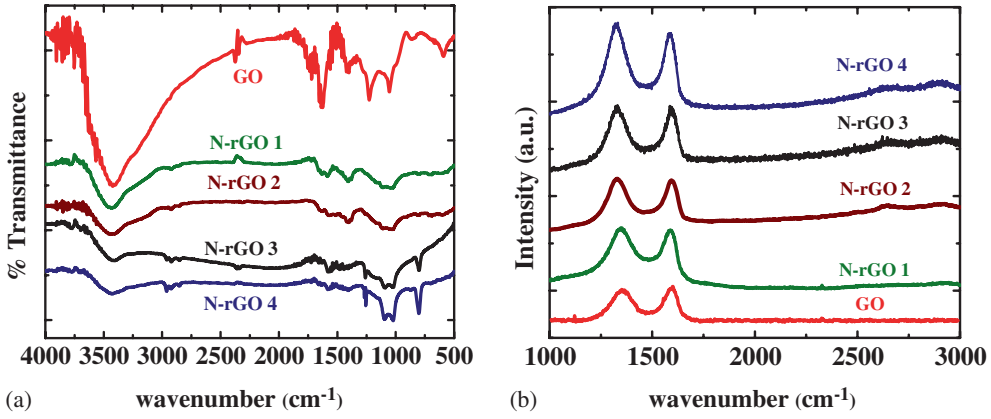

Figure 1. (a) FTIR and (b) Raman spectral profiles of GO and different N-rGOs.

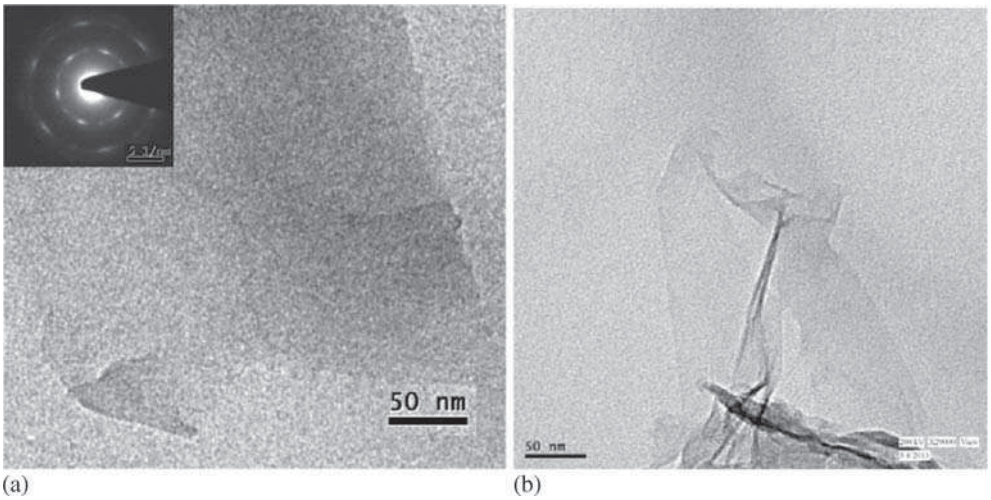

Figure 2. TEM image of N-rGO3 (a, b). The SAED pattern of the corresponding TEM image is shown in Figure 2a inset.

Table 1. Nitrogen content (N/C atomic ratio) of N-rGO samples acquired from XPS profile.*

	Pyridinic*	Pyrrolic*	Graphitic*	Pyridinic N oxide*	Total N/C ratio	C/O ratio
N-rGO 1	0.02	0.0143	0.0137	0.0042	0.052	3.4
N-rGO 2	0.028	0.022	0.012	0.003	0.065	4.44
N-rGO 3	0.040	0.018	0.013	0.003	0.074	4.56
N-rGO 4	0.044	0.0182	0.0148	0.003	0.078	5.66

*Data given here are the atomic ratio of the respective nitrogen and carbon (N/C) present in the samples.

quantitatively monitor the removal of oxygen functionalities, the C/O ratio was obtained for all N-rGOs from the XPS profiles. A steady increase in the C/O was noticed while moving from N-rGO1 to N-rGO4 (table 1). A new peak has emerged at 285.5eV for the C-N bond, indicating the doping of nitrogen onto the rGO framework. The intensity of this band for N-rGO3 and N-rGO4 is significantly high with respect to N-rGO1 and N-rGO2. The deconvoluted N1s spectra show characteristic signatures for four types of nitrogen such as pyridinic, pyrrolic, graphitic and pyridinic N oxide (figures 3 and 4).[3,11,16,17] The close examination of the XPS profiles reveal that both N-rGO3 and N-rGO4 have almost same % of pyridinic and pyrrolic nitrogens. N-rGO3 and N-rGO4 have as large as 53% of pyridinic nitrogen whereas N-rGO1 has the lowest pyridinic nitrogen of 38.5%. It is interesting to note that the N/C and C/O ratio gradually increases while increasing the concentration of reducing/doping agent, suggesting that, (i) facile doping of nitrogen and (ii) efficient removal of oxygen functionalities at high concentration of the doping/reducing agent. Moreover, we could achieve reasonably good amount of nitrogen doping with our simple chemical method.

3.2 *Electrocatalytic reduction of oxygen*

The electrocatalytic activity of N-rGOs was evaluated with cyclic and hydrodynamic voltammetry techniques. Well-defined voltammogram for ORR was obtained

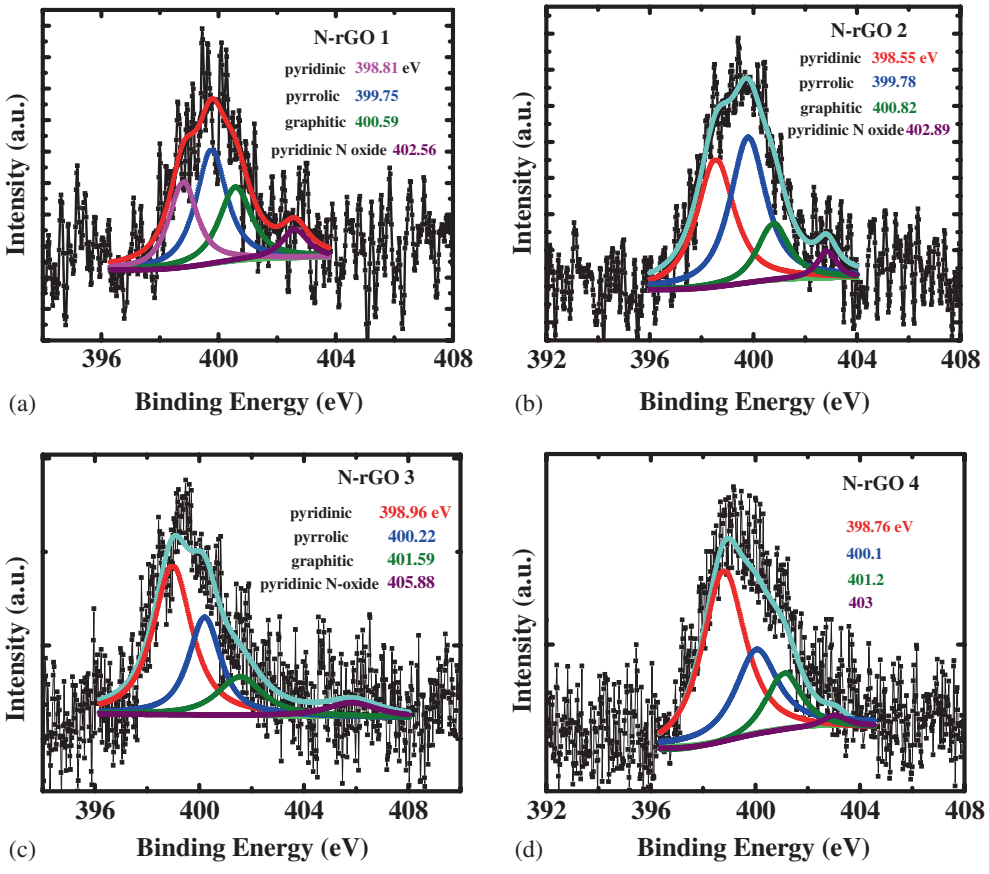

Figure 3. Deconvoluted XPS N1s spectral profiles of different N-rGOs.

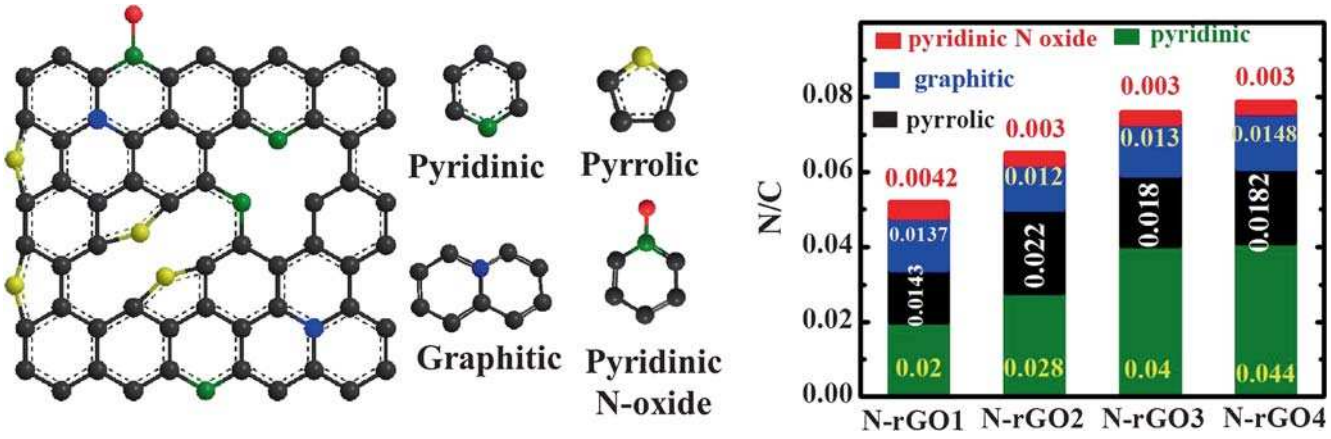

Figure 4. Four different types of nitrogen present in N-rGOs. The data given in the plot is the atomic ratio of the respective nitrogen and carbon (N/C) present in the samples.

with N-rGO3 and N-rGO4 (figures 5a and 5b). On the other hand, the voltammetric response of N-rGO1 and N-rGO2 is rather ill-defined, suggesting sluggish electron transfer kinetics. The reduction peak potential for oxygen on N-rGO3 and N-rGO4 is significantly more positive than that of N-rGO1 and N-rGO2, indicating the high electrocatalytic activity of N-rGO3 and N-rGO4. The current density on N-rGO3 and N-rGO4 is significantly higher than that of other N-rGOs. It is worth pointing out here that the undoped rGO does not show any characteristic signature for ORR (figure S5) in our experimental condition, indicating that the doped nitrogen on the rGO framework is actually responsible for the catalytic activity of N-rGO. Figure 5c is the polarization curves obtained for ORR with different N-rGOs. In all the cases, steady and gradual increase in the

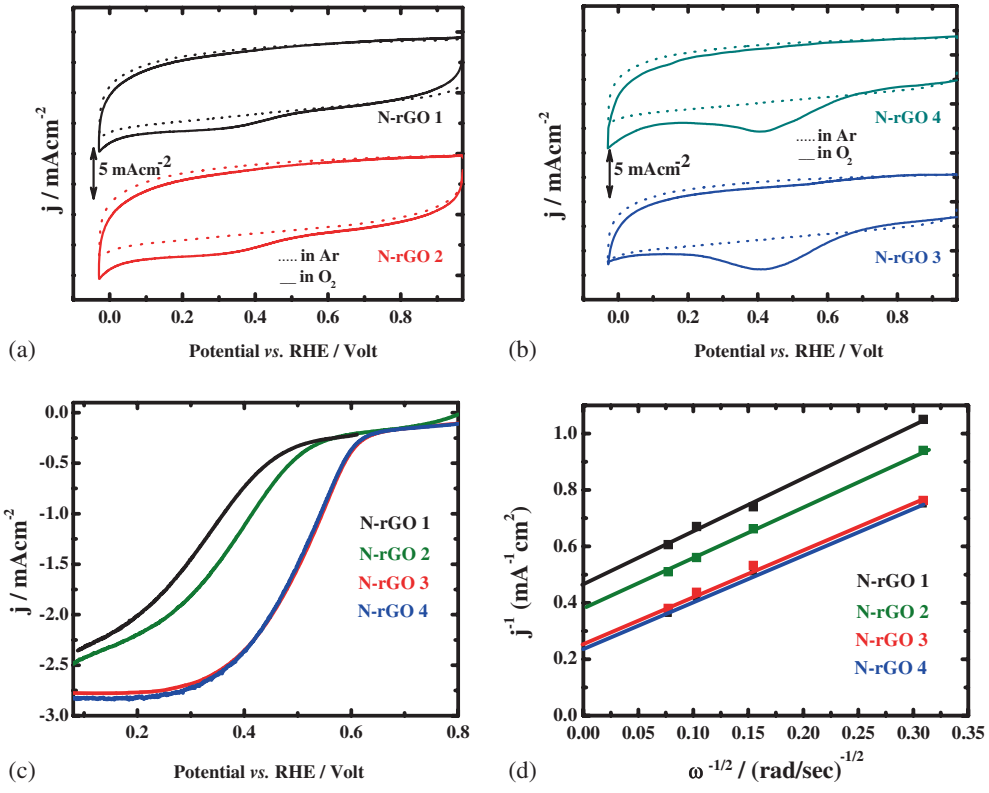

Figure 5. Cyclic voltammogram in Ar and O_2 saturated electrolyte presented by dotted and solid line, respectively, for (a) N-rGO1 and N-rGO2, (b) N-rGO3 and N-rGO4, scan rate 50 mV/s (c) Polarization curves for ORR on different N-rGO catalysts in 0.5 M H_2SO_4 solution at 1600 rpm, scan rate, 5 mV/s. (d) corresponding Koutecky-Levich plot for the different N-rGOs at 0.27 V.

limiting current was obtained while increasing the rotation. The polarization curves on N-rGO3 and N-rGO4 are better defined, suggesting facile electron transfer kinetics. As can be seen, the onset potential and the limiting current density on N-rGO3 and N-rGO4 is higher than that of the other two N-rGOs. Both N-rGO3 and N-rGO4 show almost identical limiting current density of ~2.7 mA/cm^2, which is around 1.26 times higher than the other N-rGOs at the potential of 0.17 V. The polarization curves were analyzed using Koutecky-Levich (K-L) plot according to the following equation:[7,32]

$$\frac{1}{j} = \frac{1}{j_k} + \frac{1}{j_d} \tag{1}$$

Where j is the current density, and j_K is the kinetic current density at a particular potential, j_d is the diffusion limiting current density. Linear K-L plot with similar slope was obtained at different potential (figure 5d). RRDE experiments were performed to further understand the ORR kinetics (figure S6B). The number of electrons transferred during ORR and the % of H_2O_2 generated during ORR was obtained from K-L plot and RRDE voltammograms from the following eqns. 2 and 3:[4,7,33]

$$n = \frac{4 \times I_d}{\left(I_d + \frac{I_r}{N}\right)} \tag{2}$$

$$\%H_2O_2 = 200 \times \frac{I_r}{(I_d + I_r/N)} \tag{3}$$

Here, I_d is the disk current, I_r is the ring current, and N is the geometric factor of the RRDE known as current collection efficiency of the Pt ring, which was determined to be 0.37. The number of electrons transferred for all the catalysts throughout the potential range is ~3.9 suggesting that N-rGO favors the 4-electron pathway for the reduction of oxygen. The kinetics of electrocatalytic reduction of oxygen was further analyzed by the Tafel plot. The mass transport-correcte Tafel plot (figure S7A) was made using the following equation:[33]

$$j_k = \frac{j.j_d}{j_d - j} \tag{4}$$

Tafel slope in the low current density region on N-rGO3 and N-rGO4 catalysts was calculated to be 72 mV dec^{-1} and 83 mV dec^{-1}, respectively. On the other hand, in the higher current density region, N-rGO3 and N-rGO4 has the slope of 140 and 151 mV dec^{-1}, respectively. The slopes are slightly higher than that of those of the conventional Pt-based electrocatalysts. Tafel slope obtained for our catalyst is closely similar to those reported for the natively grown nitrogen-doped graphene/porous carbon and phosphorus doped porous carbon.[34,35] Tafel slope on N-rGO1 and N-rGO2 deviates largely (higher than that of N-rGO3 and N-rGO4) from the theoretical values, presumably due to the poor oxygen adsorption and sluggish reaction kinetics. Further studies are required to quantitatively evaluate the reaction kinetics and to probe the reaction mechanism. The durability of the catalysts was studied by registering amperometric i-t curve in O_2 saturated 0.5 M H_2SO_4 (figure S7B). The potential of the electrode was biased at 0.17 V and the current was monitored for a period of 10,000 s. Only a small decrease in the current (1-3.5%) was observed for the N-rGO3 and N-rGO4 catalyst after 10,000 s, indicating the high durability of the catalyst. In the case of N-rGO1 and N-rGO2, significant loss of current was noticed.

A careful analysis of the polarization curves for ORR reveals that the electrocatalytic activity of N-rGO3 and N-rGO4 is significantly higher than that of other N-rGOs (table 2). It is worth comparing the electrocatalytic performance of our catalyst with the other nitrogen-doped electrocatalysts synthesized at various experimental conditions (table S1 in Supplementary Information). In most of the cases, the catalyst was synthesized by thermal annealing at high temperature and the onset potential falls in between 0.6 and 0.8 V. Limiting current density ranging from 1.7 to 4.5 mA/cm^2 has been achieved. In our case, we used the chemical doping method and we could achieve a current density of 2.7 mA/cm^2 with an onset potential of 0.66 V, suggesting that our catalysts have comparable electrocatalytic activity. Interestingly, Tafel slope of N-rGO3 and N-rGO4 catalyst is close to that of the Pt

Table 2. The catalytic activity for N-rGOs.

Electrocatalysts (N-rGOs)	Onset potential (V)	Kinetic current density at 0.27 V (mA/cm^2)	Current density at 0.27 V (mA/cm^2)
N-rGO1	0.55	2.2	1.64
N-rGO2	0.58	2.63	1.94
N-rGO3	0.66	4	2.71
N-rGO4	0.66	4.31	2.76

electrocatalyst. The high electrocatalytic activity can be explained by considering the type of carbon-nitrogen bond and the amount and chemical nature of nitrogen doped onto the rGO network. The change in the chemical and electronic environment can significantly influence the ORR activity of the catalyst. The exact role of different types of nitrogen in the electrocatalytic reduction of oxygen is still a matter of dispute. Some of the research groups suggest that the pyridinic nitrogen is catalytically active[36–42] whereas other groups support the involvement of graphitic nitrogen.[43,44] The contribution of both pyridinic and graphitic nitrogen in the catalytic activity cannot be ruled out.[17,45] Ruoff's group claimed that the amount of graphitic nitrogen determines the limiting current density whereas the pyridinic nitrogen play important role in improving the onset potential for ORR.[17] Our studies reveal that the pyridinic nitrogen plays key role in catalyzing ORR. As described earlier the % of pyridinic nitrogen in N-rGO3 and N-rGO4 is higher than that of the other N-rGOs. The doping of electronegative nitrogen atom onto the carbon network breaks the electroneutrality of C-C bond and change the chemical nature of graphene. Such doping polarizes the carbon atom and hence it can function as a favorable site for oxygen adsorption to facilitate the electron transfer for the reduction of oxygen. Moreover, doping of pyridinic nitrogen onto the carbon network would increase the $2p\pi$ state of C-N and diminish the C-C electron density.[46] The increase in the N/C ratio would change the density of state near the fermi level and alters the band structure for graphene framework. The N-rGO3 and N-rGO4 has more than 50% pyridinic nitrogen and they have the highest onset potential among all N-rGOs. The pyridinic type of nitrogen has the main role in deciding the catalytic activity. It has been suggested that the graphitic nitrogen actually enhances the limiting current density.[17] In our case, though all our N-rGO1 and N-rGO2 catalysts have almost same amount of graphitic nitrogen as N-rGO3 and N-rGO4, the limiting and kinetic current density and the onset potential are lower in the case of both N-rGO1 and N-rGO2. Moreover, the kinetic current density on N-rGO1 is $\sim$ 50% less than that of the N-rGO4 catalyst. Although N-rGO2 has the lowest amount of graphitic nitrogen, the limiting and kinetic current density are higher than those of N-rGO1, suggesting that the graphitic nitrogen may not have significant influence in the catalytic activity. It is considered that the pyridinic nitrogen actually promotes the catalytic activity of nitrogen-doped rGO. The C atom bonded to the pyridinic nitrogen could be the actual catalytic site. The contribution of other nitrogen may not be completely ruled out, as all the catalysts contain four different types of nitrogen. The synthetic limitation does permit the doping of rGO only with pyridinic nitrogen.

4. Conclusions

The chemical nature and nitrogen content-dependent electrocatalytic performance of nitrogen-doped reduced graphene oxide towards ORR has been investigated. It is demonstrated that the nitrogen content (N/C ratio) actually controls the electrocatalytic performance. Our study shows that the nitrogen-doped materials with more amount of pyridinic nitrogen have high electrocatalytic activity. The amount of pyridinic nitrogen actually decides the onset potential and limiting current density. The electrocatalytic performance of nitrogen-doped reduced graphene oxide can be regulated by tuning the amount of pyridinic nitrogen. Nitrogen-doped reduced graphene oxide with high N/C ratio and large amount of pyridinic nitrogen has high catalytic activity among all the catalysts. The graphitic nitrogen has limited ORR activity. The reduced graphene oxide with only pyridinic nitrogen would provide more insight into the actual catalytic site and the ORR mechanism. Further work is required to synthesize reduced graphene oxide doped only with pyridinic nitrogen and to study their catalytic activity.

Supplementary Information (SI)

Experimental details, elemental mapping, XPS survey scan, deconvoluted C1s spectra, and cyclic voltammogram are given as supplementary information. For details see www.ias.ac.in/chemsci.

Acknowledgements

This work was financially supported by Department of Science and Technology, New Delhi. We thank Department of Physics, Indian Institute of Technology Kharagpur for XPS measurements.

References

1. Nie Y, Li L and Wei Z 2015 *Chem. Soc. Rev.* **44** 2168
2. Wu G and Zelenay P 2013 *Acc. Chem. Res.* **46** 1878
3. Bag S, Roy K, Gopinath C S and Raj C R 2014 *ACS Appl. Mater. Interfaces* **6** 2692
4. Bag S, Mondal B, Das A K and Raj C R 2015 *Electrochim. Acta* **163** 16
5. Dai L, Xue Y, Qu L, Choi H J and Baek J B 2015 *Chem. Rev.* **115** 4823
6. Zhou X, Qiao J, Yang L and Zhang J 2014 *Adv. Energy Mater.* **4** 1301523
7. Ghosh S and Raj C R 2010 *J. Phys. Chem. C* **114** 10843

8. Seger B and Kamat P V 2009 *J. Phys. Chem. C* **113** 7990
9. Wei D, Liu Y, Wang Y, Zhang H, Huang L and Yu G 2009 *Nano Lett.* **9** 1752
10. Shui J, Wang M, Du F and Dai L 2015 *Sci. Adv.* **1** 140012
11. Wang H, Maiyalagan T and Wang X 2012 *ACS Catal.* **2** 781
12. Zhang J, Zhao Z, Xia Z and Dai L 2015 *Nat. Nanotechnol.* **10** 444
13. Gong K, Du F, Xia Z, Durstock M and Dai L 2009 *Science* **323** 760
14. Watanabe H, Asano S, Fujita S, Yoshida H and Arai M 2015 *Chem. Sus. Chem.* **8** 1156
15. Ma Z, Dou S, Shen A, Tao L, Dai L and Wang S 2015 *Angew. Chem.* **127** 1908
16. Rao C V, Cabrera C R and Ishikawa Y 2010 *J. Phys. Chem. Lett.* **1** 2622
17. Lai L, Potts J R, Zhan D, Wang L, Poh C K, Tang C, Gong H, Shen Z, Lin J and Ruoff R S 2012 *Energy Environ. Sci.* **5** 7936
18. Raj C R 2013 In *Innovative graphene technologies: Evaluation and application* A Tiwari and A A Balandin (Eds.) (Shropshire: Smithers Rapra Technology Ltd.) p. 293
19. Wang Y, Shao Y, Matson D W, Li J and Lin Y 2010 *ACS Nano* **4** 1790
20. Stankovich S, Dikin D A, Piner R D, Kohlhaas K A, Kleinhammes A, Jia Y, Yue Wu, Nguyen S B T and Ruoff R S 2007 *Carbon* **45** 1558
21. Park S, Hu Y, Hwang J O, Lee E S, Casabianca L B, Cai W, Potts J R, Ha H W, Chen S, Oh J, Kim S O, Kim Y H, Ishii Y and Ruoff R S 2012 *Nat. Commun.* **3** 638
22. Dey R S, Hajra S, Sahu R K, Raj C R and Panigrahi M K 2012 *Chem. Commun.* **48** 1787
23. Bag S and Raj C R 2014 *J. Mater. Chem. A* **2** 17848
24. Hummers W S and Offeman R E 1958 *J. Am. Chem. Soc.* **80** 1339
25. Gao M R, Lin Z -Y, Zhuang T -T, Jiang J, Xu Y -F, Zheng Y -R and Yu S –H 2012 *J. Mater. Chem.* **22** 13662
26. Hu C, Liu Y, Yang Y, Cui J, Huang Z, Wang Y, Yang L, Wang H, Xiao Y and Rong J 2013 *J. Mater. Chem. B* **1** 39
27. Lin Z, Waller G, Liu Y, Liu M and Wong C P 2012 *Adv. Energy Mater.* **2** 884
28. Lin Z, Waller G H, Yan L, Liu M and Wong C P 2013 *Carbon* **53** 130
29. Yang S, Zhi L, Tang K, Feng X, Maier J and Müllen K 2012 *Adv. Funct. Mater.* **22** 3634
30. Tuinstra F and Koenig J L 1970 *J. Chem. Phys.* **53** 1126
31. Rodil V S, Paredes J I, Alonso A M and Tascón J M D 2009 *J. Mater. Chem.* **19** 3591
32. Gojkovi S L, Zecevic S K and Savinell R F 1998 *J. Electrochem. Soc.* **145** 3713
33. Antoine O and Durand R 2000 *J. Appl. Electrochem.* **30** 839
34. Liang J, Du X, Gibson C, Du X W and Qiao S Z 2013 *Adv. Mater.* **25** 6226
35. Wu J, Yang Z, Li X, Sun Q, Jin C, Strasser P and Yang R 2013 *J. Mater. Chem. A* **1** 9889
36. Liu J, Song P, Zhigan N and Xu W 2015 *Electrocatalysis* **6** 132
37. Sidik R A, Anderson A B, Subramanian N P, Kumaraguru S P and Popov B N 2006 *J. Phys. Chem. B* **110** 1787
38. Zhang L and Xia Z 2011 *J. Phys. Chem. C* **115** 11170
39. Li Y, Zhao Y, Cheng H, Hu Y, Shi G, Dai L and Qu L 2011 *J. Am. Chem. Soc.* **134** 15
40. Li H, Kang W, Wang L, Yue Q, Xu S, Wang H and Liu J 2013 *Carbon* **54** 249
41. Ding W, Wei Z, Chen S, Qi X, Yang T, Hu J, Wang D, Wan L J, Alvi S F and Li L 2013 *Angew. Chem. Int. Ed.* **52** 11755
42. Tuci G, Zafferoni C, D'Ambrosio P, Caporali S, Ceppatelli M, Rossin A, Tsoufis T, Innocenti M and Giambastiani G 2013 *ACS Catal.* **3** 2108
43. Niwa H, Horiba K, Harada Y, Oshima M, Ikeda T, Terakura K, Ozaki J and Miyata S 2009 *J. Power Sources* **187** 93
44. Tiva S, Guangzhi H, Xueen J and Thomas W 2012 *ACS Nano* **6** 8904
45. Liu M, Song Y, He S, Tjiu W W, Pan J, Xia Y-Y and Liu T 2014 *ACS Appl. Mater. Interfaces* **6** 4214
46. Luo Z, Lim S, Tian Z, Shang J, Lai L, MacDonald B, Fu C, Shen Z, Yu T and Lin J 2011 *J. Mater. Chem.* **21** 8038